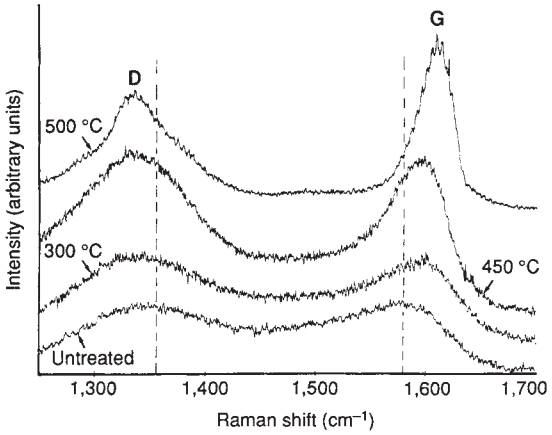

FIG. 3 Raman spectra of the LoxM-grade Tyranno fibres before and after hydrothermal treatments at various temperatures. Ar laser radiation at a wavelength of 488 nm was used. The spectra are composed of a graphite line (G) and a disorder-induced line (D). Vertical dashed lines show the predicted positions of G and D lines for polycrystalline graphite. The shift of the observed lines from 1,580 and 1,355 cm^{-1} indicates the presence of the bond-angle disorder. The up-shift of the G line towards the high-frequency edge means that the crystallites have a very small grain size, and that they are dominated by sp^2 C–C rather than sp^3 C–C bonds[22]. However, the down-shift of the D line indicates the presence of sp^3 carbon bonds as well as disorder. The decrease of the full width at half maximum of both lines with increasing temperature means the removal of the bond-angle disorder and the increasing dominance of crystallites.

sizes. Calculations of the strength of the SiC core of the fibre with film demonstrated that it was not changed after hydrothermal treatment below 450 °C.

The hydrothermal method has also potential for fabrication of amorphous carbon or graphite films on various silicon carbide substrates. Graphite films can be useful for controlling the friction between SiC and a counterbody in wear applications. Coatings on whiskers and platelets may gradually improve the fracture toughness and work of fracture of ceramic matrix composites. Treatment of fine SiC powders can produce carbon-coated particles which undergo sintering more readily. The presence of a carbon film on the surface allows the electrical resistivity of Tyranno fibres to be varied from 1 to 10^6 Ω cm, making possible their use in resistive cables. Hydrothermal treatment for longer times and/or at higher temperatures, that leads to full consumption of the fibre core, results in the formation of very thin, hollow carbon pipes with an outer diameter of <10 μm and wall thickness of ~3 μm. Such carbon structures might be of interest for specific applications such as catalysis. Further investigation of the properties of the carbon films is necessary, however, to identify their ideal applications. Preliminary experiments with TiC, TaC, WC and NbC show that the surface modification of other carbides by formation of carbon, or carbon containing, layers is also possible. □

Received 27 September; accepted 21 December 1993.

1. Tsai, H. & Bogy, D. B. *J. Vac. Sci. Technol.* A**5,** 3287–3312 (1987).
2. Jones, R. H., Schilling, C. H. & Schoenlien, L. H. *Materials Science Forum* Vol. 46 277–308 (Trans Tech, Aedermannsdorf, Switzerland, 1989).
3. Fischbach, D. B. & Lemoine, P. M. *Composites Sci. Technol.* **37,** 55–61 (1990).
4. Li, J. X., Matsuo, Y. & Kimura, S. *Bull. ceram. Soc. Japan* **99,** 1207–1211 (1991).
5. Chaim, C. & Heuer, A. H. *Adv. Ceram. Mater.* **2,** 154–158 (1987).
6. Sōmiya, S. (ed.) *Hydrothermal Reactions for Materials Science and Engineering* (Elsevier, London, 1989).
7. Hirano, S.-I., Nakamura, K. & Sōmiya, S. in *Hydrothermal Reactions for Materials Science and Engineering* (ed. Sōmiya, S.) 331–336 (Elsevier, London, 1989).
10. Rumble, D., Duke, E. F. & Hoering, T. L. *Geology* **14,** 452–455 (1986).
11. Rumble, D. & Hoering, T. C. *Geochim. cosmochim. Acta* **50,** 1239–1247 (1986).
12. Yoshimura, M., Kase, J.-I. & Sōmiya, S. *J. Mater. Res.* **1,** 100–103 (1986).
13. Hirayama, H., Kawakubo, T., Goto, A. & Kanako, T. *J. Am. ceram. Soc.* **72,** 2049–2053 (1989).
14. Kanno, Y., Yasuda, E. & Yoshimura, M. *J. Surf. Sci. Soc. Japan* **14,** 229–235 (1993).
15. Yamamura, T. *et al.* in *Looking Ahead for Materials and Processes* (eds de Bossu, J., Briens, G. & Lissac, P.) 19–28 (Elsevier, Amsterdam, 1987).
16. Cooke, T. F. *J. Amer. ceram. Soc.* **74,** 2959–2978 (1991).
17. Kajiyoshi, K., Ishizawa, N. & Yoshimura, M. *J. Am. ceram. Soc.* **74,** 369–374 (1991).
18. Gonzalaz-Hernandez, J., Chao, B. S. & Pawlik, D. A. *J. Vac. Sci. Technol.* A**7,** 2332–2338 (1989).
19. Tuinstra, F. & Koenig, J. L. *J. chem. Phys.* **53,** 1126 (1970).
20. Eriksson, G. *Chemica Scripta* **8,** 100 (1975).
21. Ito, S. & Tomozawa, M. *J. Am. ceram. Soc.* **64,** 160 (1981).
22. Wang, W., Wang, T. & Chen, B. *J. appl. Phys.* **72,** 69–72 (1992).

ACKNOWLEDGEMENTS. We thank M. Kakihana for help with Raman spectroscopy, T. Yamamura for providing Tyranno fibres, M. Shibuya for assistance with AES and TEM analysis, and G. Burkhard for discussions. One of us (Yu.G.) was supported by a JSPS Research Fellowship.

Total synthesis of taxol

K. C. Nicolaou*†, Z. Yang*, J. J. Liu*, H. Ueno*, P. G. Nantermet*, R. K. Guy*, C. F. Claiborne*, J. Renaud*, E. A. Couladouros*, K. Paulvannan* & E. J. Sorensen*†

* Department of Chemistry, The Scripps Research Institute, 10666 North Torrey Pines Road, La Jolla, California 92037, USA
† Department of Chemistry, University of California, San Diego, 9500 Gilman Drive, La Jolla, California 92093, USA

TAXOL[1–4], a substance originally isolated from the Pacific yew tree (*Taxus brevifolia*) more than two decades ago, has recently been approved for the clinical treatment of cancer patients. Hailed as having provided one of the most significant advances in cancer therapy[5], this molecule exerts its anticancer activity by inhibiting mitosis through enhancement of the polymerization of tubulin and consequent stabilization of microtubules[6]. The scarcity of taxol and the ecological impact of harvesting it have prompted extensive searches for alternative sources including semisynthesis, cellular culture production and chemical synthesis[2,3]. The latter has been attempted for almost two decades, but these attempts have been thwarted by the magnitude of the synthetic challenge. Here we report the total synthesis of taxol by a convergent strategy, which opens a chemical pathway for the production of both the natural product itself and a variety of designed taxoids.

The strategy for the present synthesis of taxol (**1**, Fig. 1*a*) was based on a retrosynthetic analysis involving the bond disconnections[7] shown in Fig. 1*b*. Thus, in the synthetic direction the following key operations were proposed: (1) two fragments, representing precursors to rings A and C (see Fig. 1*a*), were to be coupled by a Shapiro reaction[8] and a McMurry coupling[9] to assemble the ABC ring skeleton; (2) instalment of the oxetane ring; (3) addition[10] of the various substituents around the peripheries of rings B and C; (4) oxygenation[10] at C-13; and (5) esterification to attach the side chain[11].

The previously reported intermediates **2** (ref. 12) (Fig. 2) and **8** (refs 7, 13) (Fig. 3) served as the starting points for the convergent synthesis of taxol reported here. Figure 2 presents the construction of the requisite C-ring aldehyde **7** from **2**. Protection of both hydroxyl groups in **2** with TBS groups (95%) (for abbreviations see figure legend) followed by selective reduction of the ester group with $LiAlH_4$ at 0 °C, furnished primary alcohol **3** (94% yield). Acid-catalysed deprotection of the secondary alcohol in **3** proceeded in a highly selective manner to give the corresponding diol (90% yield), which was then selectively protected with a TPS group at the primary position and a benzyl group at the secondary to afford compound **4** in 80% overall

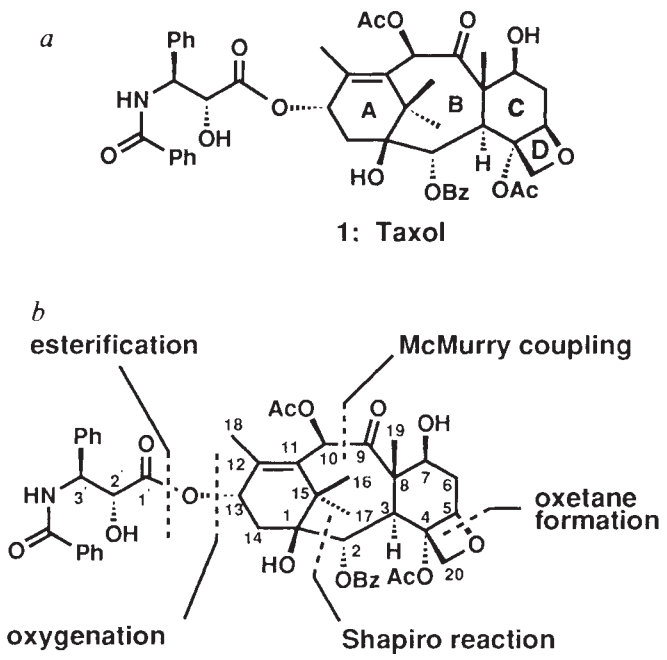

FIG. 1 Structure (*a*) and strategic bond disconnections of taxol (*b*). Abbreviations for chemical groups (see also Figs 2, 3 and 5): Ph, phenyl; OBz, benzoyl; OAc, acetyl.

25 °C to produce triol **5** in 80% yield. Finally, acetonide formation followed by TPAP[14] oxidation in the presence of NMO resulted in the formation of the targeted aldehyde **7** in 80% overall yield.

Figure 3 summarizes the coupling of intermediates **7** and **8** and elaboration of the coupling product to give the requisite tricyclic system **13**. When the vinyl lithium reagent derived from aryl hydrazone **8** and *n*-C_4H_9Li (refs 8, 13) was reacted with aldehyde **7** at −78 °C, a single diastereoisomer of hydroxy-compound **9** was obtained in 82% yield. Directed epoxidation of the C1–C14 double bond in **9** was realized, in 87% yield, using *t*-C_4H_9OOH in the presence of $VO(acac)_2$ (ref. 15), leading selectively to epoxide **10** which was regioselectively opened with $LiAlH_4$ to give the 1,2-diol **11** (76% yield). X-ray crystallographic analysis of this compound (**11**) confirmed the designated stereochemistry for intermediates **9–11** and their relatives (Fig. 4*a*). To prepare the molecule for closure of the 8-membered B ring, and in order to create subsequent opportunities for the introduction of the benzoate functionality at C-2, diol **11** was converted to its cyclic carbonate by exposure to phosgene in the presence of KH, furnishing dialdehyde **12**, after desilylation (*n*-$(C_4H_9)_4NF$) and oxidation (TPAP-NMO)[14] in 32% overall yield. The suitably preorganized dialdehyde **12** was then subjected to a McMurry-type[9,13] cyclization to afford the taxoid ABC ring system **13** in 23% yield (stereochemistry at the newly generated centres assigned by X-ray crystallographic analysis of a subsequent intermediate, **13′**; see below and Fig. 4*c*).

The next important intermediate in the synthesis was **19**, a compound that was reached from **13** as outlined in Fig. 5. Monoacetylation of **13** followed by oxidation with TPAP-NMO[14] furnished, regioselectively in 88% overall yield, ketoacetate **14**. The stereochemistry of the acetate group at C-10 was confirmed through conversion of **14** to the crystalline benzoate **14′** (PCC, $NaO(CO)CH_3$, celite, benzene, heat) and X-ray crystallographic analysis on the latter (see ORTEP drawing, Fig. 4*b*). Hydroboration of compound **14** followed by basic hydrogen peroxide treatment led to a mixure of two regioisomeric alcohols (55%, ~3:1 by ^1H NMR) which was subjected to acid-induced removal of the acetonide group and chromatographic separation to afford triol **15** (33% yield from **14**) as the major product. The primary hydroxyl group in **15** was then selectively acetylated under standard conditions, furnishing compound **16** in 95% yield. At this stage the benzyl protecting group on the C-7 oxygen was replaced by a triethyl silyl group (TES) for reasons arising from later stages of the synthesis, and the resulting compound was selectively monodeacetylated under mildly basic conditions (K_2CO_3-CH_3OH) leading to triol **17** (78% overall yield). The oxetane ring was finally constructed by sequential monosilylation with TMSCl (primary OH), triflate formation (secondary OH) and mild acid treatment to afford, after acetylation of the remaining tertiary hydroxyl group, the targeted intermediate **19** in 38% overall yield[16]. Racemic **19**, obtained from this sequence, was identical in all respects (except for optical rota-

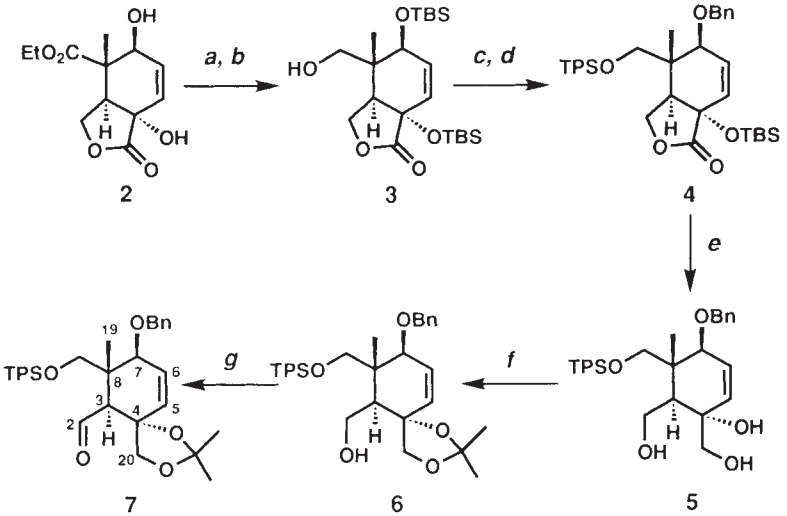

FIG. 2 Construction of C-ring system **7**. Reagents and conditions. (*a*) *t*-$BuMe_2SiOTf$ (4 equivalents (eq.)), 2,6-lutidine (4 eq.), 4-DMAP (0.01 eq.), CH_2Cl_2, 0 °C, 4 h, 95%; (*b*) $LiAlH_4$ (1.1 eq.), Et_2O, 0 °C, 1 h, 94%; (*c*) (1) CSA (0.05 eq.), MeOH, CH_2Cl_2, 25 °C, 1 h, 90%; (2) t-$BuPh_2SiCl$ (1.5 eq.), imidazole (1.6 eq.), DMF, 25 °C 6 h, 92%; (*d*) KH (1.2 eq.), Et_2O, *n*-Bu_4NI (cat.), BnBr (1.2 eq.), 25 °C, 2 h, 87%; (*e*) $LiAlH_4$ (3 eq.), Et_2O, 25 °C, 12 h, 80%; (*f*) 2,2-dimethoxypropane (5 eq.), CSA (0.1 eq.), CH_2Cl_2, 25 °C, 7 h 82%; (*g*) TPAP (0.05 eq.), NMO (1.5 eq.), CH_3CN, 25 °C, 2 h, 95%. (Bn = CH_2Ph; CSA = (±)-camphorsulphonic acid; 4-DMAP = 4-dimethylaminopyridine; DMF = N,N-dimethylformamide; NMO = N-methylmorpholine-N-oxide; TBS = *t*-$BuMe_2Si$; TPAP = tetra-*n*-propylammonium perruthenate; TPS = *t*-$BuPh_2Si$.) Selected physical data for compound **7**: ^1H NMR (500 MHz, $CDCl_3$, taxol numbering): δ 9.98 p.p.m. (d, J = 3.5 Hz, 1 H, 2-H), 7.65–7.12 (m, 15 H, aromatic), 5.84 (dd, J = 10.5, 1.5 Hz, 1 H, 6-H), 5.71 (dd, J = 10.5, 2.0 Hz, 1 H, 5-H), 4.50 (d, J = 11.5 Hz, 1 H, OCH_2Ph), 4.22 (d, J = 11.5 Hz, 1 H, OCH_2Ph), 4.20 (d, J = 9.5 Hz, 1 H, 20-H), 4.10 (dd, J = 2.0, 1.5 Hz, 1 H, 7-H), 3.84 (d, J = 9.5 Hz, 1 H, 20-H), 3.72 (d, J = 10.0 Hz, 1 H, 9-H), 3.70 (d, J = 10.0 Hz, 1 H, 9-H), 3.18 (d, J = 3.5 Hz, 1 H, 3-H), 1.42 (s, 3 H, CH_3-acetonide), 1.39 (s, 3 H, CH_3-acetonide), 1.09 (s, 9 H, $(CH_3)_3$ CSi), 1.04 (s, 3 H, 19-CH_3); ^{13}C NMR (125 MHz, $CDCl_3$): δ 202.3, 138.1, 135.8, 135.6, 133.0, 132.9, 131.1, 129.7, 129.4, 129.5, 128.8, 128.2, 127.6, 127.4, 127.4, 127.2, 127.2, 1,720.4, 1,111.5 cm $^{-1}$; high resolution mass spectrometry (fast atom bombardment) (HRMS (FAB)): calcd for $C_{36}H_{44}O_5Si$ (M^+ + Cs) mass-to-charge ratio m/z = 607.2856 atomic mass units (a.m.u.) found

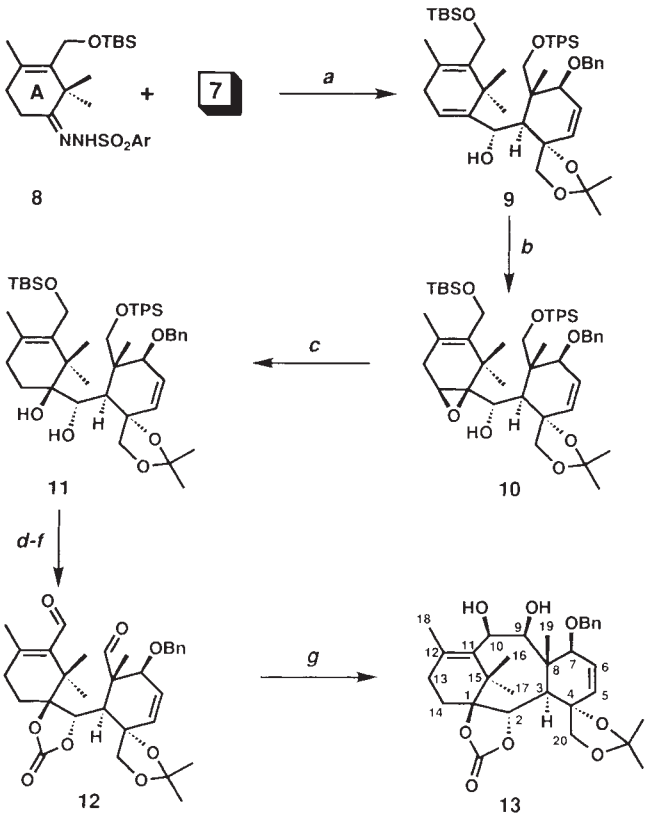

FIG. 3 Construction of ABC ring system 13. Reagents and conditions. (*a*) (1) **8**, *n*-BuLi (2.05 eq.), THF, −78 °C → 25 °C, cool to 0 °C and add **7** (1.0 eq. in THF), 0.5 h, 82%; (*b*) $VO(acac)_2$ (0.03 eq.), *t*-BuOOH (3 eq.), 4-Å molecular sieve (cat.), benzene, 25 °C, 12 h, 87%; (*c*) $LiAlH_4$ (3 eq.), Et_2O, 25 °C, 7 h, 76%; (*d*) KH (3 eq.), HMPA/Et_2O (30/70), $COCl_2$ (20% in benzene, 2 eq.), 25 °C, 2 h, 48%; (*e*) TBAF (10 eq.), THF, 25 °C, 7 h, 80%; (*f*) TPAP (0.05 eq.), NMO (3 eq.), CH_3CN/CH_2Cl_2 (2:1), 25 °C, 2 h, 82%; (*g*) $(TiCl_3)_2$–$(DME)_3$ (10 eq.), Zn–Cu (20 eq.), DME, 70 °C, 1 h, 23%. Ar = 2,4,6-triisopropylbenzene sulphonyl; HMPA = hexamethyl-phosphoric triamide; NMO = 4-methylmorpholine-N-oxide; TBAF = tetra-*n*-butylammonium fluoride; TBS = *t*-$BuMe_2Si$; TPAP = tetra-*n*-propylammonium perruthenate. Selected physical data for compound **13**: ^1H NMR (500 MHz, $CDCl_3$, taxol numbering): δ 7.42–7.31 (m, 5 H, aromatic), 5.97 (dd, J = 10.0, 1.5 Hz, 1 H, 5-H), 5.63 (dd, J = 10.0, 1.5 Hz, 1 H, 6-H), 5.46 (d, J = 5.0 Hz, 1 H, 2-H), 4.77 (d, J = 12.0 Hz, 1 H, OCH_2Ph), 4.49 (d, J = 8.5 Hz, 1 H, 20-H), 4.39 (d, J = 12.0 Hz, 1 H, OCH_2Ph), 4.29 (d, J = 5.5 Hz, 1 H, 10-H), 4.24 (d, J = 5.5 Hz, 1 H, 9-H), 3.80 (d, J = 8.5 Hz, 1 H, 20-H), 3.58 (b, 1 H, 7-H), 2.75–2.71 (m, 1 H, 13-H), 2.61–2.50 (m, 1 H, 13-H), 2.34 (d, J = 5.0 Hz, 1 H, 3-H), 1.98–1.92 (m, 1 H, 14-H), 1.83–1.74 (m, 1 H, 14-H), 1.58 (s, 3 H, 18-CH_3), 1.45 (s, 3 H, 19-CH_3), 1.42 (s, 3 H, CH_3-acetonide), 1.41 (s, 3 H, CH_3-acetonide), 1.19 (s, 3 H, 16-CH_3), 1.08 (s, 3 H, 17-CH_3); ^{13}C NMR (125 MHz, $CDCl_3$): δ 153.9, 139.4, 137.3, 136.1, 135.6, 128.7, 128.5, 128.3, 122.0, 108.2, 93.4, 82.4, 77.9, 75.7, 74.2, 71.2, 70.4, 69.3, 46.3, 44.3, 40.0, 31.2, 29.6, 28.9, 27.9, 26.8, 23.6, 21.7, 21.3, 16.0; infrafred (pure compound): ν_{max} 2,970.3, 1,789.1, 1,455.6, 1,100.3 cm^{-1}; HRMS (FAB) calcd for $C_{31}H_{40}O_8$ ($M^+ + Cs$), m/z = 673.1778 a.m.u., found 673.1782 a.m.u.

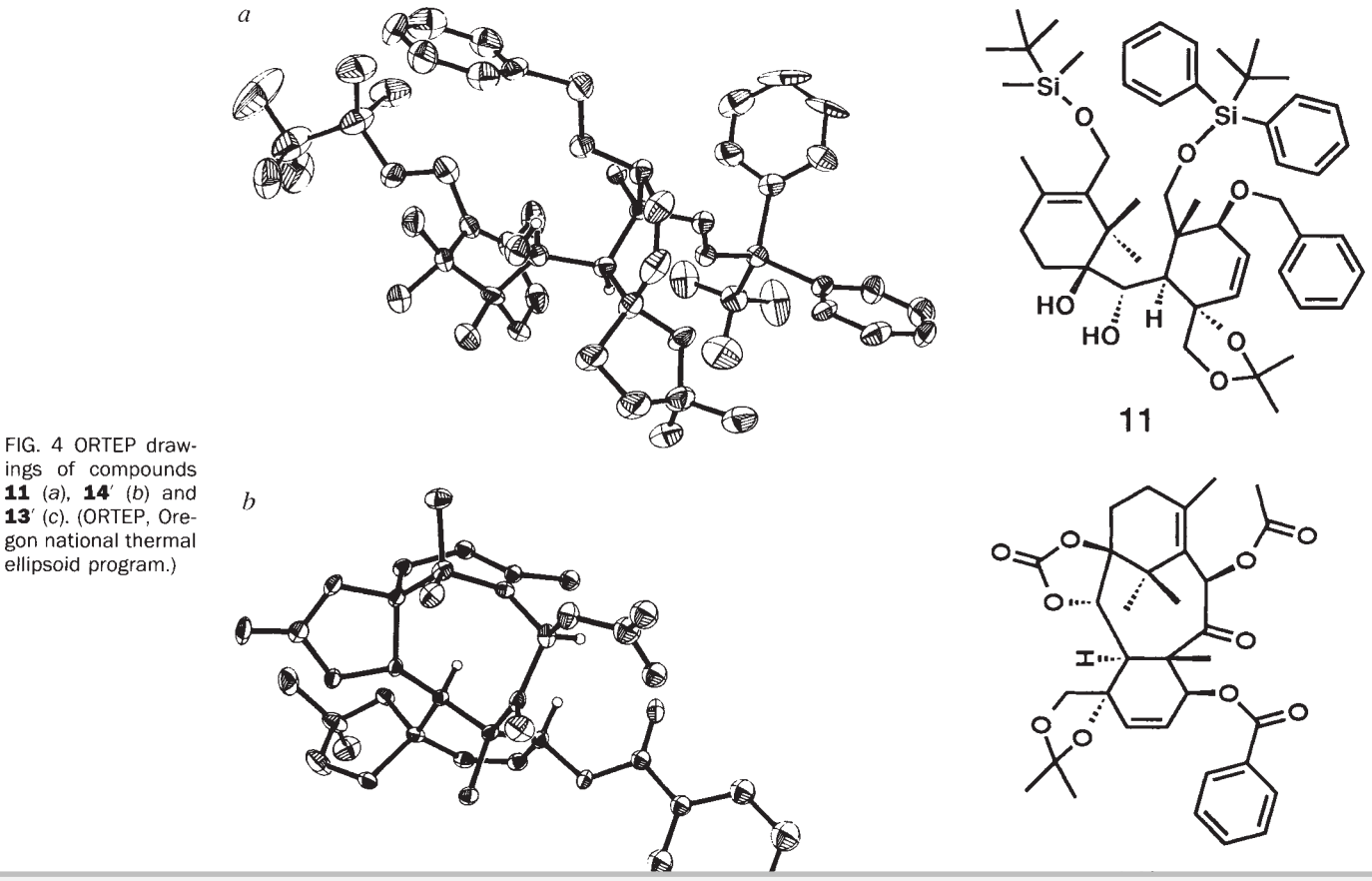

FIG. 4 ORTEP drawings of compounds **11** (*a*), **14**′ (*b*) and **13**′ (*c*). (ORTEP, Oregon national thermal ellipsoid program.)

FIG. 5 Total synthesis of ABCD ring system **19** and taxol (**1**). Reagents and conditions. (*a*) Ac_2O (1.5 eq.), 4-DMAP (1.5 eq.), CH_2Cl_2, 25 °C, 2 h, 95%; (*b*) TPAP (0.1 eq.), NMO (3 eq.), CH_3CN, 25 °C, 2 h, 93%; (*c*) BH_3–THF (5.0 eq.), THF, 0 °C, 2 h then H_2O_2, aqueous $NaHCO_3$, 0.5 h, 55% (~3:1 mixture of C5–C6 regioisomers by ^1H NMR); (*d*) conc. HCl, MeOH, H_2O, 25 °C, 5 h 80%; (*e*) Ac_2O (1.5 eq.), 4-DMAP (1.5 eq.), CH_2Cl_2, 25 °C, 0.5 h, 95%; (*f*) H_2, 10% $Pd(OH)_2$(C), EtOAc, 25 °C, 0.5 h, 97%; (*g*) Et_3SiCl (25 eq.), pyridine, 25 °C, 12 h, 85%; (*h*) K_2CO_3 (10 eq.), MeOH, 0 °C, 15 min., 95%; (*i*) Me_3SiCl (10 eq.), pyridine (30 eq.), CH_2Cl_2, 0 °C, 15 min., 96%; (*j*) Tf_2O (15 eq.), *i*-Pr_2NEt (30 eq.), CH_2Cl_2, 25 °C, 0.5 h 70%; (*k*) CSA (cat.), MeOH, 25 °C, 10 min., then silica gel, CH_2Cl_2, 25 °C, 4 h, 60%; (*l*) Ac_2O (10 eq.), 4-DMAP (20 eq.), CH_2Cl_2, 25 °C, 4 h, 94%; (*m*) (1) PhLi (5 eq.), THF, −78 °C, 10 min., 80%; (2) PCC (30 eq.), NaOAc, celite, benzene, reflux, 1 h, 75%; (3) $NaBH_4$ (10 eq.), MeOH, 25 °C, 5 h, 83%; (4) $NaN(SiMe_3)_2$ (3.5 eq.), β-lactam **20**, THF, 0 °C, 87%, based on 90% conversion; (5) HF-pyridine, THF, 25 °C, 1.5 h, 80%. (CSA = (±)-camphorsulphonic acid; 4-DMAP = N-dimethylaminopyridine; NMO = 4-methylmorpholine-N-oxide; TPAP = tetra-*n*-propylammonium perruthenate. Selected physical data for compound **19**: ^1H NMR (500 MHz, $CDCl_3$, taxol numbering): δ 6.40 (s, 1 H, 10-H), 4.95 (d, J = 9.0 Hz, 1 H, 5-H), 4.60 (d, J = 9.0 Hz, 1 H, 20-H), 4.47 (d, J = 9.0 Hz, 1 H, 20-H), 4.43 (dd, J = 10.0, 7.5 Hz, 1 H, 7-H), 4.39 (d, J = 5.5 Hz, 1 H, 2-H), 3.36 (d, J = 5.5 Hz, 1 H, 3-H), 2.71 (m, 1 H, 13α-H), 2.56 (m, 1 H, 6-H), 2.17 (s, 3 H, OAc), 2.15 (s, 3 H, OAc), 2.12 (m, 1 H, CH_2), 2.07 (s, 3 H, 18-CH_3), 1.97 (m, 1 H, CH_2), 1.88 (m, 2 H, CH_2), 1.78 (s, 3 H, 19-CH_3), 1.23 (s, 3 H, 16-CH_3), 1.17 (s, 3 H, 17-CH_3), 0.88 (t, J = 7.5 Hz, 9 H, $Si(CH_2CH_3)_3$, 0.55 (dq, J = 8.0, 3.0 Hz, 6 H, $Si(CH_2CH_3)_3$; ^{13}C NMR (125 MHz, $CDCl_3$); δ 202.6, 170.3, 169.2, 153.1, 144.0, 130.7, 92.8, 84.0, 80.3, 80.0, 76.4, 76.1, 60.3, 43.5, 38.0, 29.7, 29.4, 25.5, 23.1, 21.9, 21.1, 19.1, 9.8, 6.7, 5.2; infrared (pure compound) ν_{max} 2,924, 1,814, 1,728, 1,461, 1,372, 1,238 cm^{-1}; HRMS (FAB) calcd for $C_{31}H_{46}O_{10}Si$ (M^+ + Cs) m/z = 739.1915 a.m.u., found 739.1929 a.m.u.

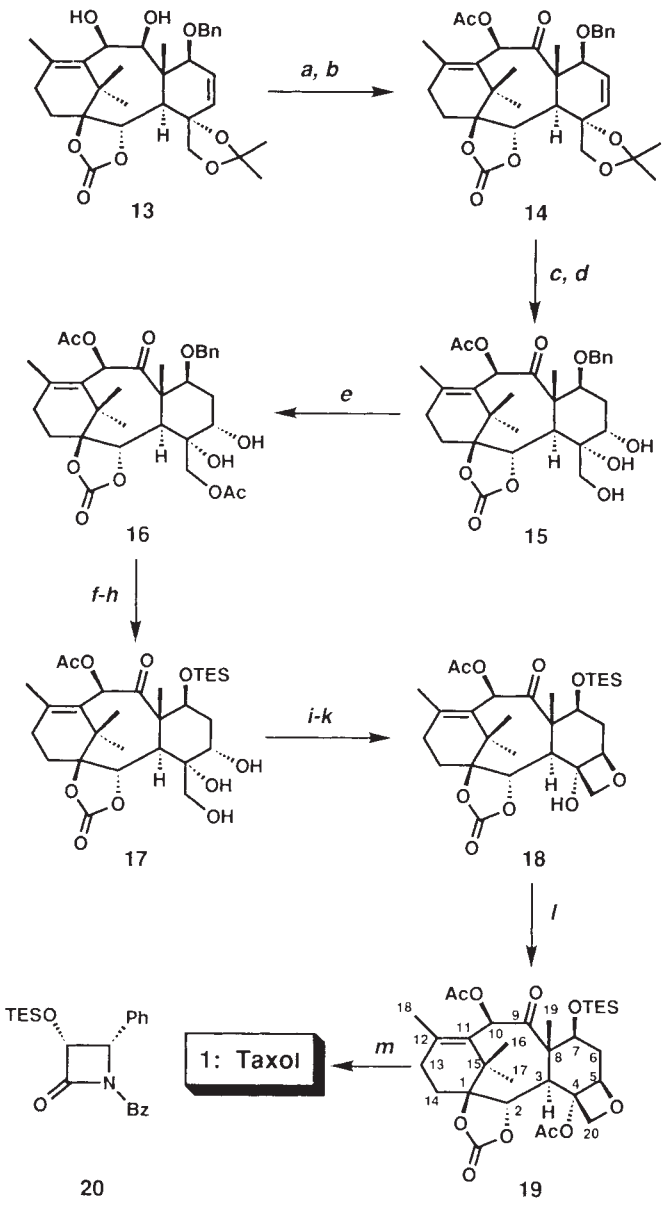

tion) with an authentic sample generated from taxol (**1**) or 10-deacetyl baccatin III (ref. 17) as described elsewhere[10]. Optically active **19** was obtained by the same route using enantiomerically pure diol **13** secured by resolution with 1(S)-(−)-camphanic chloride. Thus, reaction of racemic **13** with 1(S)-(−)-camphanic chloride gave, in 86% total yield, two diastereoisomers (**13′** and **13″**) which were chromatographically separated and characterized by X-ray crystallographic analysis on one of them (more polar isomer, silica gel, 15% $C_2H_5O(CO)CH_3$ in benzene, R_F = 0.21) (see ORTEP drawing for **13′**, antipode to desired enantiomer; Fig. 4*c*). Optically pure **13** ($[\alpha]_D^{22}$ + 187°($CHCl_3$, *c* 0.5)) was then generated from the correct diastereoisomer (**13″**, less polar, silica gel, 15% $C_2H_5O(CO)CH_3$ in benzene, R_F = 0.26) by exposure to methanolic K_2CO_3 (90% yield).

The conversion of enantiomerically pure **19** to taxol (**1**) followed the sequence[10]: (1) excess C_6H_5Li, −78 °C to regioselectively open the carbonate ring and afford the desired hydroxybenzoate functionality (80%); (2) PCC-$NaO(CO)CH_3$, benzene, reflux to introduce a carbonyl group at C-13 (75%); (3) excess $NaBH_4$-CH_3OH to stereospecifically generate the C-13 hydroxyl group (83%); (4) $NaN(Si(CH_3)_3)_2$ then Ojima's β-

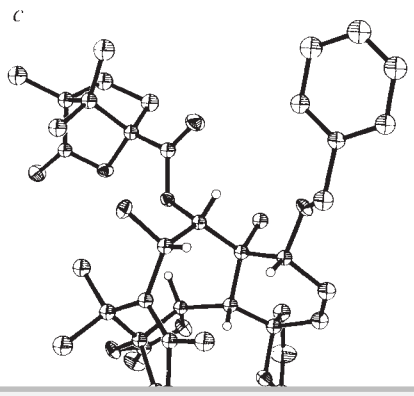

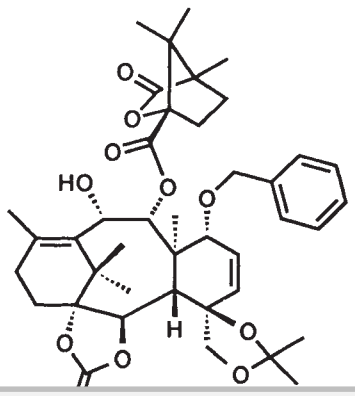

lactam (**20**)[11], 0 °C, to attach the side chain (87% yield based on 90% conversion); and (5) HF–pyridine, to remove the silyl groups (80%). Synthetic taxol was found to be identical in all respects with naturally occurring taxol, including spectroscopic characteristics (^{1}H and ^{13}C NMR, infrared spectroscopy, mass spectra, $[\alpha]_D^{22}$) and biological activity (microtubule stabilization and cytotoxicity against Molt-4 leukaemia cells).

The chemistry described here not only offers a solution to a formidable synthetic challenge but also opens a completely chemical avenue to taxol, other naturally occurring taxoids and synthetic, designed taxoid derivatives. □

Received 24 January, accepted 31 January 1994.

1. Wani, M. C., Taylor, H. L., Wall, M. E., Coggon, P. & McPhail, A. T. *J. Am. chem. Soc.* **93,** 2325–2327 (1971).
2. Nicolaou, K. C., Dai, W.-M. & Guy, R. K *Angew. Chem. int. Edn engl.* **33,** 15–44 (1994).
3. Guenard, D., Gueritte-Voegelein, F. & Poitier, P. *Acct Chem. Res.* **26,** 160–167 (1993).
4. Rowinksy, E. K., Cazenave, L. A. & Donehower, R. C. *J. natn. Cancer Inst.* **82,** 1247–1259 (1990).
5. *Paclitaxel (Taxol) Investigations Workshop Semin. Oncol.* **20** (4, Suppl. 3), 1–60 (1993).
6. Schiff, P. B., Fant, J. & Horwitz, S. B. *Nature* **277,** 665–667 (1979).
7. Nicolaou, K. C., Hwang, C.-K., Sorensen, E. J. & Claiborne, C. F. *J. chem. Soc., chem. Commun.* 1117–1118 (1992).
8. Chamberlin, A. R. & Bloom, S. H. *Org. React.* **39,** 1–83 (1990).
9. McMurry, J. E. *Chem. Rev.* **89,** 1513–1524 (1989).
10. Nicolaou, K. C., Nantermet, P. G., Ueno, H. & Guy, R. K. *J. chem. Soc., chem. Commun.* 295–296 (1994).
11. Ojima, I. *et al. Tetrahedron* **48,** 6985–7012 (1992).
12. Nicolaou, K. C., Liu, J. J., Hwang, C.-K., Dai, W.-M. & Guy, R. K. *J. chem. Soc., chem. Commun.* 1118–1120 (1992).
13. Nicolaou, K. C., Yang, Z., Sorensen, E. J. & Nakada, M. *J. chem. Soc., chem. Commun.* 1024–1026 (1993).
14. Griffith, W. P., Ley, S. V. *Aldrichimica Acta.* **23,** 13–19 (1990).
15. Sharpless, K. B. & Verhoeven, T. R. *Aldrichimica Acta*, **12,** 63–74 (1979).
16. Magee, T. V., Bornmann, W. G., Isaacs, R. C. A. & Danishefsky, S. J. *J. org. Chem.* **57,** 3274–3276 (1992).

ACKNOWLEDGEMENTS. We thank I. Ojima for a sample for β-lactam **20**, E. Bombardelli for a gift of 10-deacetyl baccatin III, R. Chadha for the X-ray crystallographic analysis and W. Wrasidlo for the biological assays. This work was supported by the NIH, The Scripps Research Institute, fellowships from Mitsubishi Kasei Corporation (H.U.), Rhone-Poulene Rorer (P.G.N.), The Office of Naval Research (R.K.G.), Glaxo, Inc. (C.F.C.), Mr Richard Staley (C.F.C.), NSERC (J.B.R.), The Agricultural University of Athens (E.A.C.), R. W. Johnson—ACS Division of Organic Chemistry (E.J.S.), and grants from Merck Sharp and Dohme, Pfizer, Inc. and Schering Plough. Z.Y. and J.J.L. contributed equally to this project.

Model assessment of the role of natural variability in recent global warming

R. J. Stouffer, S. Manabe & K. Ya. Vinnikov

Geophysical Fluid Dynamics Laboratory/NOAA, Princeton University, Princeton, New Jersey 08542, USA

SINCE the late nineteenth century, the global mean surface air temperature has been increasing at the rate of about 0.5 °C per century[1–3], but our poor understanding of low-frequency natural climate variability has made it very difficult to determine whether the observed warming trend is attributable to the enhanced greenhouse effect associated with increased atmospheric concentrations of greenhouse gases[4,5]. Here we evaluate the observed warming trend using a 1,000-year time series of global temperature obtained from a mathematical model of the coupled ocean–atmosphere–land system. We find that the model approximately reproduces the magnitude of the annual to interdecadal variation in global mean surface air temperature. But throughout the simulated time series no temperature change as large as 0.5 °C per century is sustained for more than a few decades. Assuming that the model is realistic, these results suggest that the observed trend is not a natural feature of the interaction between the atmosphere and oceans. Instead, it may have been induced by a sustained change in the thermal forcing, such as that resulting from changes in atmospheric greenhouse gas concentrations and aerosol loading.

The coupled model[6] consists of general circulation models of (see Fig. 1 for the model description.) This model has been used for other studies of climate variability[7] and to study the transient response of climate to a gradual increase of greenhouse gases in the atmosphere[6,8–10]. The model is integrated over a 1,000-yr period, keeping unchanged all thermal forcing factors such as the solar constant, atmospheric carbon dioxide concentration. The initial condition for the integration has realistic seasonal and geographical distributions of sea surface temperature, sea surface salinity and sea ice thickness, with which both atmospheric and oceanic components of the model are nearly in equilibrium.

When the time integration of the model starts from an initial condition, the model state drifts towards its own equilibrium. To reduce this artificial drift from realistic surface conditions, the fluxes of heat and water at the ocean–atmosphere interface are adjusted by amounts which vary seasonally and geographically, but do not change from one year to the next[6]. Because these adjustments are independent of the anomalies of surface temperature and salinity, they neither damp nor amplify these anomalies.

The time series of the globally averaged, annual mean temperature obtained from the 1,000-yr integration (Fig. 1*a*) has a small trend of −0.023 °C per century. This small linear trend in the time series of global mean surface air temperature of the model is removed in the analysis to follow. This trend is <5% of the trend (0.52 °C per century) in the time series of observed, global mean surface air temperature obtained by Jones and Wigley[2] (Fig. 1*b*). In model time series, there are periods during which the rate of the warming trend is as large as 0.5 °C per century, but these periods last only a few decades.

The power spectrum of detrended, globally averaged, annual mean surface air temperature from the 1,000-yr integration of the coupled model is compared to the spectrum of detrended time series of observed temperature[2] for the period AD 1881–1990 (Fig. 2). The detrending of the observed time series removes most of the contribution from fluctuations on timescales longer than 50 yr. At interdecadal or shorter timescales, the spectrum from the coupled model is not significantly different from the spectrum of observed temperature, although the model estimate is somewhat lower than the observed particularly over the interval of 2 to 5-yr periods. As noted by Lau *et al.*[11], this low-resolution model underestimates markedly the magnitude of the Southern Oscillation on interannual timescales. If the contribution from the Southern Oscillation is removed[12] from the detrended observed time series, the standard deviation is 0.101 °C. This compares favourably to the standard deviation (0.096 °C), of the detrended time series from the model. Thus, with the exception of the interannual variations associated with the Southern Oscillation, it appears that the coupled model used here approximately reproduces the observed variability of the global mean temperature on annual to interdecadal timescales.

To assess the probability of finding a century-scale warming trend such as that observed between AD 1881 and 1990 in the time series from the coupled model, we calculated the fraction of occurrence for linear trends (calculated over various time intervals) exceeding 0.5 or 0.25 °C per century (Fig. 3). As the time interval over which the trend is calculated grows longer, the fraction of occurrence becomes smaller. For intervals longer than ~60 yr, there are no trends as large as 0.5 °C per century; for intervals longer than ~90 yr, there are no trends as large as 0.25 °C per century. Therefore the observed warming trend of 0.52 °C per century is not found in the coupled model time series for any intervals longer than ~60 yr. The standard deviation of the linear trend calculated over 110-yr intervals from the detrended time series from the coupled model is ~0.07 °C per century, and is much smaller than the observed warming trend. Although a small trend of 0.023 °C per century is removed from the time series as discussed earlier, the effect of this detrending on the analysis described here is small. In short, it is not very